Journal of Photochemistry & Photobiology, B: Biology 208 (2020) 111901

Contents lists available at ScienceDirect

Journal of Photochemistry & Photobiology, B: Biology

journal homepage: www.elsevier.com/locate/jphotobiol

NIR-dye based mucoadhesive nanosystem for photothermal therapy in breast cancer cells

Anil Jogdand[1], Syed Baseeruddin Alvi[1], P.S. Rajalakshmi, Aravind Kumar Rengan*

Department of Biomedical Engineering, Indian Institute of Technology Hyderabad, Telangana 502285, India

ARTICLE INFO

Keywords:
Niosome,IR 806
Mucoadhesive nanosystem
Breast cancer
Photothermal therapy

ABSTRACT

Breast cancer is one of the leading causes of mortality in women, worldwide. The average survival rate of patients suffering from advanced breast cancer is about 27% for five years. Photothermal therapy employing biodegradable nanoparticle are extensively researched for enhanced anticancer therapy in breast cancer treatment. In the current study, we report a chitosan based mucoadherant and biodegradable niosome nanoparticle entrapping near infrared (NIR) dye (IR 806) for the treatment of breast cancer. Niosome entrapping IR 806 (NioIR) showed encapsulation efficacy of about 56 ± 2%. The prepared nanoparticles (NioIR) were further coated with chitosan (NioIR-C) to impart mucoadhesive property to the nanosystem. NioIR-C showed minimal degradation following NIR laser irradiation, thus enhancing its photothermal stability. They also exhibited efficient photothermal transduction, when compared with IR 806 dye. NioIR-C were biocompatible when treated with normal cell lines (NIH 3T3 and L929) and showed cytotoxicity towards breast cancer cell lines (MCF-7 and MDA-MB 231). When triggered with NIR laser, NioIR-C showed photothermal cell death (approximately 93%). The presence of chitosan coating on NioIR led to mucoadherence potential that further enhances the therapeutic effect on breast cancer cells when compared with IR 806 dye and NioIR. Thus NioIR-C can be a promising nanosystem for effective treatment of breast cancer using photothermal therapy.

1. Introduction

Breast carcinoma is one of the most prominent heterogeneous tumors found in women. It accounts for about 14.7% of cancer-related deaths [1]. The various treatment modalities include surgery (mastectomy), chemo and radiation therapy. All these therapies are known to exhibit various adverse effects [2,3]. Among the current strategies under research, Photothermal therapy (PTT) is considered as a promising approach for the treatment of cancer. PTT employs NIR laser (650 nm to 950 nm) that has minimal interference with biological tissue, thereby achieving an increased depth of penetration [4]. In PTT, the nanoparticles absorb NIR light; the absorbed light is then converted to heat which is employed to kill cancer cells [5].

The plasmon resonant nanoparticles and the NIR dyes are used for achieving an optimal photothermal effect. For this purpose, hydrophilic and hydrophobic dyes are extensively being researched for their potential therapeutic benefits [6–8]. Among hydrophilic NIR dyes, Indocyanine Green (ICG) is an FDA approved contrast agent for imaging in clinical applications [9]. However, its application is limited due to instability in an aqueous environment, concentration dependent aggregation, rapid degradation and clearance from the body [10].

IR 806 is one of the hydrophilic negatively charged NIR dye. The sulfonate functional group on IR 806 increases its water solubility; it also prevents dye aggregation and exhibits reduced cellular uptake [11,12]. According to recent literature, IR 806 dye exhibits enhanced photothermal effect when encapsulated within silica nanoparticles [13]. However, silica nanoparticles exhibit minimal degradation and delayed clearance from the body, limiting its clinical translation [14]. Hydrophobic NIR dyes are reported for photothermal therapy, but they are known to exhibit potential long-term systemic toxicity [15]. Both hydrophilic and hydrophobic NIR-dyes in their free state has limitations due to various reasons such as photobleaching, photodegradation, low bioavailability, non-specificity to cancer cells, etc. [16]. To overcome these limitations, various research groups have formulated delivery systems that are stable, site-specific, and exhibit enhanced therapeutic efficacy [17,18]. The drug delivery to cancer site is affected due to various factors like dense tumor-microenvironment, interstitial pressure, etc. [19,20]. These factors prevent the accumulation of drug at the tumor site reducing its therapeutic efficacy. Hence newer strategies are developed to enhance the penetration and retention of the drug via

* Corresponding author at: Department of Biomedical Engineering, Indian Institute of Technology Hyderabad, Telangana 502285, India.
E-mail address: aravind@bme.iith.ac.in (A.K. Rengan).
[1] Authors contributed equally.

https://doi.org/10.1016/j.jphotobiol.2020.111901
Received 18 September 2019; Received in revised form 27 March 2020; Accepted 15 May 2020
Available online 20 May 2020
1011-1344/

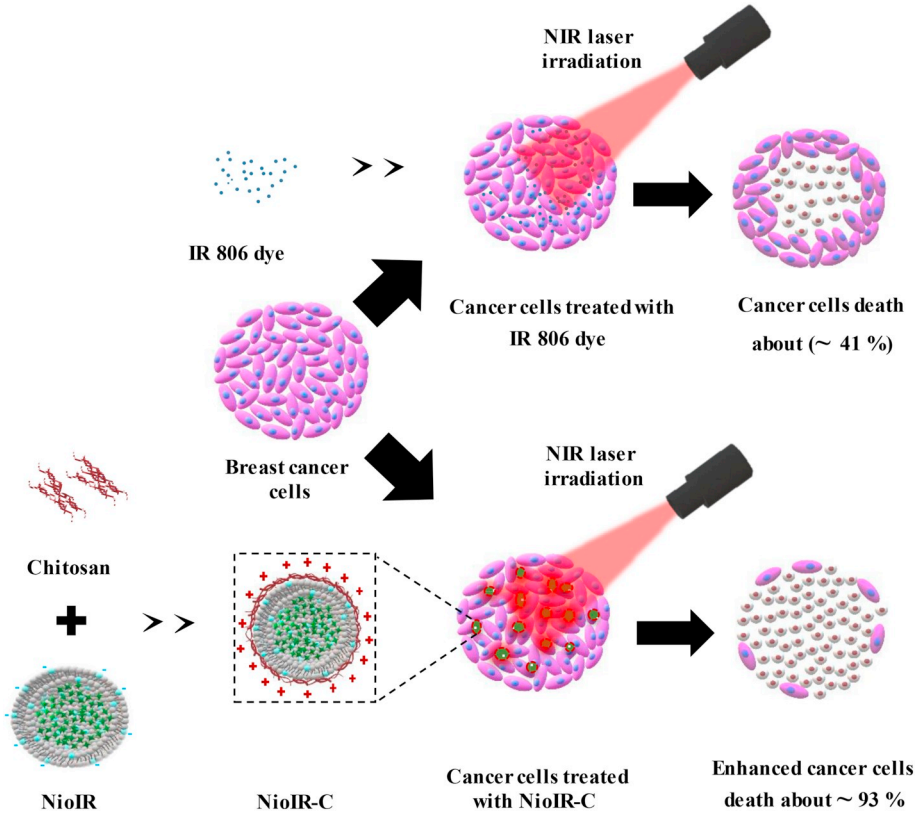

Scheme 1. Schematic of NioIR-C Mediated Photothermal Therapy of Breast Cancer Cells

nanoparticle system within the tumor matrix [21].

In breast cancer, the extracellular matrix is enriched with glycoproteins like mucins; these glycoproteins are responsible for poor drug penetration and play a major role in evading immune response [22–24]. Inhibition of mucin expression in breast cancer models has shown to significantly enhance the therapeutic efficacy of the treatment [25]. The glycoproteins within the tumor matrix can be targeted by mucoadherant nanosystem that can enhance its localized availability and prevent its rapid clearance.

In the current study, chitosan coated biodegradable non-ionic surfactant based bilayer vesicles (Niosome) are used as a delivery vehicle for IR 806 dye to enhance its therapeutic outcome (Scheme 1).

2. Materials and Methods

2.1. Materials

Sorbitan monopalmitate (SPAN 40), Dihexadecyl phosphate (DCP), IR 806 dye, Chitosan (low molecular weight) were purchased from Sigma (St. Louis, MO, USA). Cholesterol, 3-(4, 5-Dimethylthiazol-2-yl)-2, 5-Diphenyltetrazolium Bromide (MTT). Nile red and solvents: Methanol, Chloroform, Dimethyl sulfoxide (DMSO), Triton X-100 were procured from SRL chemicals, India. Phosphate buffer saline (PBS) pH 7.0, Trypsin-EDTA, Dulbecco's Modified Eagle Media(DMEM), Fetal Bovine Serum (FBS) (US origin), were purchased from Hi-media Chemicals, Mumbai, India. 0.2-μm syringe filters were obtained from Sartorius (Carrigtwohill, Ireland). All the chemicals were used as obtained without any further purification.

2.2. Cell Lines and Maintenance

Human breast adenocarcinoma (MCF- 7 and MDA-MB 231), Mouse embryonic fibroblast (NIH 3 T3) and Murine fibroblast L929, were obtained from the Centre for Cellular and Molecular Biology (CCMB), Hyderabad, India. The cell lines were cultured in DMEM medium supplemented with 10% (*v*/v) Fetal bovine serum (FBS), 1% L-Glutamine, and 100 U/ml penicillin/streptomycin and were maintained at 37 °C in a humidified atmosphere containing 5% CO^2.

2.3. Preparation of Niosomes Entrapping IR 806 (NioIR)

The niosomes were prepared by solvent injection method with minor modifications [26–28]. Briefly, 1 mg IR 806 dye was dissolved in 2 ml Milli-Q water. SPAN 40, Cholesterol and DCP have weighed accurately as mentioned in Table S1 and dissolved into 1 ml chloroform, and the resulting solution was taken into a syringe and injected into a beaker containing 3 ml of IR 806 dye solution maintained at 60 °C at 500 RPM for 1 h. Synthesized niosomes were further sonicated using 150 W probe sonicator at 30% for 10 min and dialyzed (cut off 14,000 Da) for 36 h to remove the unentrapped IR 806 dye.

2.4. Preparation of Chitosan Coated NioIR (NioIR-C)

Chitosan solution was prepared by dissolving chitosan in 1% acetic acid solution (3 mg/ml). The chitosan coating on NioIR was obtained by dropwise addition of NioIR to chitosan solution (10:1 *w*/w) with vigorous stirring. The obtained solution was stirred for 12 h and sonicated using 150 W for 10 min then further dialyzed for 24 h to remove uncoated free chitosan [29,30].

2.5. Characterization of NioIR and NioIR-C

The absorbance and fluorescence of nanoparticles was measured by UV Spectrophotometer (UV-1800, Shimadzu, Japan) and Spectrofluorophotometer (RF-6000, Shimadzu, Japan) respectively. The hydrodynamic diameter, polydispersity index (PDI) and zeta potential were measured by particle size analyzer (Particle Sizing Systems, Inc. Santa Barbara, Calif., USA). Surface topography and size were

analyzed by Atomic force microscopy (Dimension Icon, Bruker). The NioIR-C were imaged by Transmission Electron Microscopy (TEM) (JEOL, JEM 2100, USA).

2.6. IR 806 Dye Encapsulation Efficiency (EE) and Loading Capacity (LC) Quantification

The IR 806 dye solution (1 mg/ml) was prepared in 0.1% Triton X-100 and was further diluted to different concentrations (0.25, 0.5, 1, 2, 3, and 4 μg/ml). The absorbance of each dilution was measured by UV spectrophotometer at λ max 820 nm, and the calibration curve was plotted. The linear regression equation was obtained from the calibration curve of the IR 806 dye ($x = \frac{y - 0.0137}{0.2854}$, $R^2 = 0.9997$). The encapsulation efficacy of synthesized NioIR was measured using UV spectrophotometer by dissolving it in 0.1% of Triton X-100, which disrupts the vesicle. Encapsulation efficiency (EE%) of IR 806 dye in NioIR was calculated by using the formulas [31,32].

$$EE\% = \frac{\text{IR 806 dye encapsulated}}{\text{The total amount of IR 806 dye}} \times 100$$

Loading capacity (LC%) of IR 806 dye was calculated by using the formula [31,32]:

$$LC\% = \frac{\text{Weight of IR 806 dye}}{\text{The total Weight of NioIR}} \times 100$$

2.7. Investigation of the Laser-Mediated Dye Degradation Profile

IR 806, NioIR and NioIR-C (5 μg/ml in water) were irradiated with 808 Laser (Shanghai Inter-Diff Optoelectronics Technology Ltd., Shanghai, China) (650 mW) for 100 s. Absorption spectra were recorded using UV Spectrophotometer at 10 s. interval. Recorded absorbance v/s time was plotted for the respective material.

2.8. Photothermal Transduction Efficacy Studies

To study the Photothermal transduction efficiency of IR 806, NioIR and NioIR-C (300 μl, 50 μg/ml) were taken in 96 well plates and were subjected to laser irradiation for 10 min. Phosphate buffer saline (PBS) was used as control. The temperature of these solutions was recorded during NIR laser irradiation with a thermal imaging camera. Thermal images corresponding to various time points and their respective temperatures were captured by the thermal camera (CHAUVIN ARNOUX, C.A. 1950 DiaCAm IR CAMERA IP 54 Paris, France). The temperature increment was plotted against time for all the samples.

2.9. Mucin Binding Assay

The muco-adhesive property of the NioIR and NioIR-C was studied by mucin binding assay [29]. Briefly, Mucin solution (1 mg/ml) was prepared in PBS (pH 7.4) and mixed with the NioIR and NioIR-C in the ratio 1:1 (*v*/v). The mixture was incubated at 37 °C for 3 h. The suspension was then centrifuged at 15,000 rpm for 1 h, and the supernatant was collected, diluted and analyzed using UV spectrophotometer for the amount of unbound mucin at λ max, 205 nm. The concentration of free mucin was calculated from the mucin calibration curve. The amount of adsorbed mucin to the NioIR and NioIR-C was calculated by the difference between the initial amount of mucin, and the free mucin recovered from the supernatant. The mucoadhesive efficiency of the NioIR and NioIR-C was calculated using the below equation:

$$\%\text{Mucoadhesive efficacy} = \frac{Co - Cf}{Co} \times 100$$

where C_0 is the initial concentration of mucin and C_f is the concentration of free mucin in the supernatant.

2.10. Artificial Mucosa Mimetic Surface (AMMS) Based Mucoadhesive Potential of NioIR-C

To analyse the mucoadhesive potential of NioIR-C, artificial mucosa mimetic surface(AMMS) was fabricated with slight modification [33]. The experiment was performed in two steps which are as follows

2.10.1. Fabrication of Artificial Mucosa Mimetic Membrane (AMMM) and Sample Film

Eggshell membrane (ESM) was obtained by dissolving the outer calcium carbonate shell in 40% glacial acetic acid (*v*/v) and subsequently washed with distilled water. The as obtained ESM was air dried by placing it on a double sided adhesive tape. 100 μl of mucin solution (4%) was applied evenly on the ESM and air-dried to form AMMM. The sample films were prepared by drop casting 100 μg of IR 806, NioIR and NioIR-C in a circular disc (0.8 cm) of aluminium foil and were air-dried.

2.10.2. Experimental Setup

The prepared sample films were allowed to interact with the membranes for 5 min. Following the incubation period, the assembly was inversely placed on a 100 mm petri-dish filled with distilled water. The samples were placed on the petri-dish such that constant contact between the surface of the sample film and the distilled water was ensured throughout the experiment. The interaction between AMMM and the sample film was monitored continuously for film detachment from the membrane and was recorded. The images were captured at varying time intervals.

2.11. Biocompatibility Studies

Mouse embryonic fibroblast (NIH 3 T3) and Murine fibroblast (L929), are used for biocompatibility studies. MTT assay was performed to study the cytotoxicity of IR 806 dye, NioIR, and NioIR-C [34]. In brief, cells were seeded in 96 well plate with a density of 1×10^4 cells/well in DMEM medium (100 μl) for 24 h. After 24 h incubation, media was replaced with fresh media containing (100 μl, 50 μg/ml IR 806 dye) IR 806, NioIR, and NioIR-C concentration. Cell viability was assessed by MTT assay.

2.12. Cellular Uptake of IR 806, NioIR, and NioIR-C

To evaluate the intracellular uptake of IR 806, (IR 806, NioIR, NioIR-C) in MCF-7 cells were quantified using Spectrofluorophotometer [31]. The cells were seeded in 6 well plates at an estimated density of 1×10^5 cells/well. The following day, media was replaced, and IR 806 dye, NioIR, and NioIR-C was added containing 50 μg/ml doses of IR 806 dye and were incubated with cells for 5 h. The cells were washed twice with PBS and trypsinized at the stipulated period. The cells were counted and later pelleted down by centrifuging at 1200 rpm for 5 min. 1 ml of methanol was added and incubated for 1 h at room temperature to extract the intracellular IR 806 dye, IR 806 dye extracted in methanol was centrifuged at 10,000 rpm for 10 min at 4 °C. The supernatants were evaluated for fluorescence (Ex: 806 nm, Em: 829 nm). The concentration of the IR 806 dye extracted was extrapolated on the standard curve (methanol) and normalized with the number of cells per well.

2.13. Fluorescence Imaging of Intracellular Uptake of Nile Red (NR) Encapsulated NioIR and NioIR-C

To evaluate the intracellular uptake of Nile Red (NR) was used as a fluorescent marker, it is encapsulated into NioIR and NioIR-C. Nile Red and IR806, NioIR (with NR), NioIR-C (with NR) in MCF-7 cells were imaged using fluorescence microscopy (Olympus CKX53) [35]. The cells were seeded in 6-well plates at an estimated density of 1×10^5 cells/well. The following day, media was replaced and NR dye, NioIR-NR, and NioIR-NR-C was added containing 10 ng/ml doses of Nile Red,

and 50 μg/ml does of IR 806 dye were incubated with cells for 5 h.

2.14. Laser-Mediated Cytotoxicity Studies

Human breast adenocarcinoma MCF-7 and MDA-MB 231 were used for laser-mediated cytotoxicity studies. MTT assay was performed to evaluate the cytotoxicity of IR 806 dye, NioIR, NioIR-C [34]. In brief, Human breast adenocarcinoma MCF-7 and MDA-MB 231 cells were seeded separately in 96-well plates (0.5×10^4 cells/ well) and grown in DMEM medium (100 μl) for 24 h. Following the incubation, the media was then replaced with fresh media containing IR 806, NioIR, and NioIR-C (50 μg/ml, IR 806 dye). 6 h of incubation period was given, following which, cells were irradiated with 808 nm laser (650 mW) for 5 min and incubated for 12 h. Cell viability was assessed by MTT assay.

2.15. In Vitro Imaging

2.15.1. Acridine Orange (AO) and Propidium Iodide (PI) Staining

AO/PI staining was performed to assess the live/dead cells [36]. Briefly 0.5×10^4 cell/well were plated in a 96 well plate. The cells were treated with IR 806 dye, NioIR, and NioIR-C; the treated cells were subjected to laser irradiation for 5 min. Following laser irradiation, the treated cells were incubated with AO/PI to stain live and dead cells, respectively. Fluorescence imaging was performed using a fluorescence microscope.

2.15.2. Alcian Blue Staining

Alcian blue staining was performed on a 90% confluent monolayer of MCF-7. Later cells were serum-starved for 12 h followed by treatment of IR 806 dye, NioIR, and NioIR-C. The treated cells were subjected to laser irradiation for 5 min. The following day cells were fixed by using glutaraldehyde and stained with alcian blue. Cells were imaged using a light microscope [37,38].

3. Results and Discussion

Niosomes entrapping IR 806 dye (NioIR) with varying concentrations of Span 40 and cholesterol were prepared by solvent injection method (Table S1). Among these formulations "F3" exhibited encapsulation efficacy of about 56 ± 2% and loading capacity of about 5.07 ± 0.46% as shown in Table S1. The formulation F3 was selected for further characterization based on its higher entrapment efficacy. The prepared niosomes (NioIR) were made to interact with chitosan (NioIR-C) for surface coating. The DCP embedded within the niosome membrane interacts with chitosan resulting in a uniform surface coating [29]. These nanoparticles were further subjected to spectrophotometric evaluation, as shown in Fig. 1A. IR 806 dye, NioIR and NioIR-C exhibited prominent absorbance at 799 nm. IR 806 dye showed its characteristic peak at 799 nm and 724 nm, but when entrapped in niosome, a blue shift was observed from 724 nm to 672 nm. Furthermore, chitosan coating on NioIR-C showed a redshift of about 10 nm from 724 nm to 734 nm with an additional peak at 917 nm, suggesting the interaction between chitosan and IR 806 dye [39]. These nanoparticles were subjected to fluorescence analysis, and the results show that the fluorescence of the IR 806 dye was quenched after encapsulation. The fluorescence quenching could be due to the aggregation of dye in the aqueous interiors of the niosomes. These findings are in corroboration to the earlier reports suggesting the aggregate formation of cyanine based dyes when encapsulated in the liposomes [40,41]. The reduction in the fluorescence intensity was found to be about 1.4 and 1.7 folds in NioIR and NioIR-C, respectively, when compared with IR 806 dye (Fig. 1 B). To further confirm the aggregate formation in the niosome, the nanoparticles entrapping IR 806 dye were disrupted in methanol. As shown in Fig. 1 B, the fluorescence of the dye was recovered in all the samples; this further confirms the reversible self-quenching of IR 806 dye in the aqueous interior of niosomes [42].

The nanoparticles were subjected to size analysis and as shown in Fig. 2 A,B NioIR and NioIR-C exhibited the hydrodynamic diameter of about 99.5 ± 42 nm (PDI: 0.178) and 180 ± 93) nm (PDI: 0.305), respectively. The difference in size was attributed to the presence of chitosan on the surface of the nanoparticle. The surface charge analysis exhibited a significant alteration in charge from −25 ± 16 mV (NioIR) to 12.1 ± 12 mV (NioIR-C) respectively (Fig. 2 C). The charge reversal of the nanosystem further confirms chitosan coating on negatively charged NioIR templates. These findings are in line with earlier reports suggesting the surface charge reversal effect [26].

NioIR and NioIR-C were subjected to TEM analysis, and as shown in Fig. 3 A,B, Fig. S1 A,B NioIR was found to be around 97 ± 45 nm whereas after chitosan coating size of particle increased to about 141 ± 76 nm. Moreover, the chitosan coating on the surface of the nanoparticles was observed. The morphology was further confirmed by AFM analysis, and as shown in Fig. 3 C,D.

In the current study, both NioIR and NioIR-C showed prominent IR 806 dye retention within the system leading to enhanced stability of the nanoformulation (Fig. S2 A). IR 806 dye, NioIR and NioIR-C were then assessed for photothermal transduction efficacy by irradiating NIR laser (808 nm, 650 mW). A significant increase in the temperature was observed in all the samples. However, in IR 806 dye, the temperature increment was less than 42 °C (essential to cause cell death) by the end of 5 min. (Fig. 4 A). This reduction of photothermal transduction efficacy could be due to degradation of IR 806 dye (exhibited by the change in colour from blue-green to the green of irradiated samples as shown in Fig. 4 B and Fig. S2, B. Whereas, in NioIR and NioIR-C, a significant enhancement of photothermal transduction was observed when compared with IR 806 dye. However, NioIR-C reached temperature beyond 45 °C within 1 min of laser irradiation and was able to maintain the elevated temperature for about 5 min of continuous laser exposure (Fig. 4 A,C). The plausible reason for enhancing the photothermal effect could be due to the conversion of NIR light to heat rather

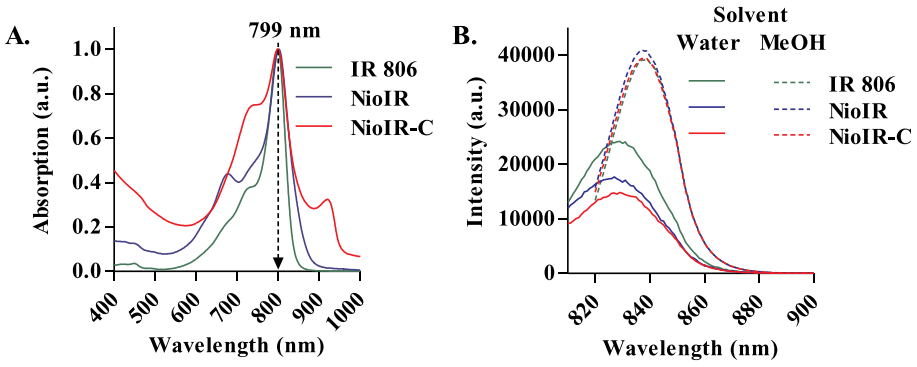

Fig. 1. A. UV–Visible absorption spectra for IR 806, NioIR, and NioIR-C.; B. Fluorescence spectrometric analysis in water and methanol of IR 806, NioIR, and NioIR-C.

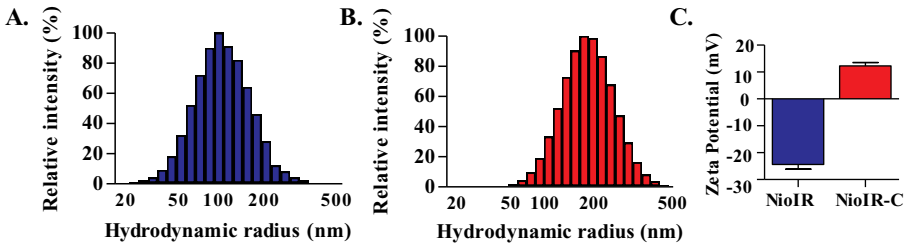

Fig. 2. Bar graphs representing hydrodynamic radius and zeta potential A. NioIR; B. NioIR-C; C. Zeta potential of NioIR and NioIR-C.

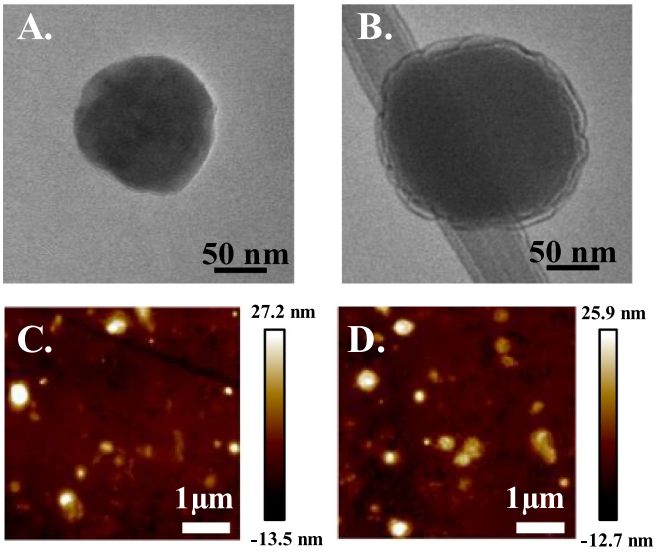

Fig. 3. Transmission electron microscopy (TEM) imaging of, A. NioIR; B. NioIR-C.; Atomic force microscopy imaging (AFM)of, C. NioIR; D. NioIR-C.

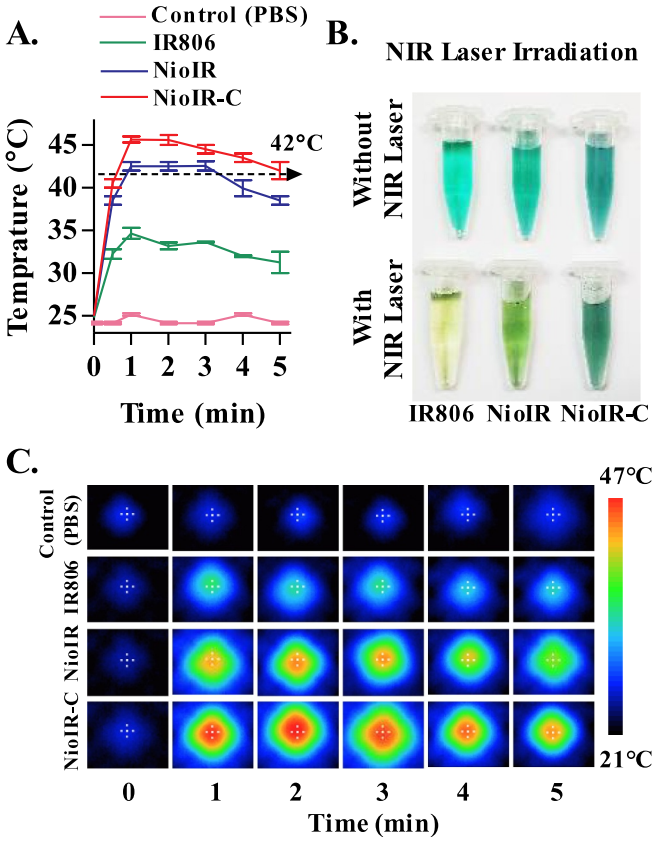

Fig. 4. Laser mediated photothermal transduction studies for IR 806, NioIR, and NioIR-C. A. line graph representing time v/s temp. After laser irradiation up to 5 min., B. Photographic images of IR 806, NioIR, and NioIR-C before and after laser irradiation; C. IR thermal imaging of IR 806 dye, NioIR, and NioIR-C at varying time interval.

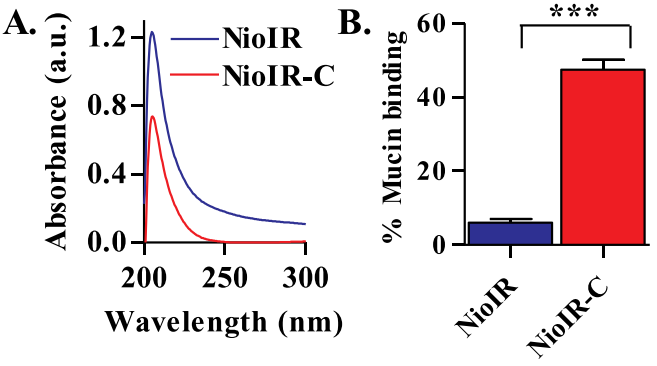

Fig. 5. Mucin binding assay for NioIR and NioIR-C. A. Line graph of unbound mucin (wavelength v/s absorbance (a.u.). B. Bar graph representing % bound mucin to NioIR and NioIR-C (*** $P < .001$).

than fluorescence and stability of IR 806 dye within NioIR-C. These findings are in agreement with the earlier literature reports suggesting that the light absorbed by the fluorophore (IR 806 dye) is dissipated as heat when its fluorescence is quenched [43].

The efficacy of NioIR-C was compared with similar hydrophilic cyanine dyes like IR783 and ICG to assess the generality of the nanosystem. As shown in Fig. S3 A, the NioIR 783-C and NioICG-C exhibited spectral changes after encapsulation in the chitosan coated niosome as seen in NioIR-C (Fig. 1 A), suggesting the generality of the niosome system towards cyanine dye. Furthermore, similar fluorescence quenching was seen in NioIR 783-C and NioICG-C (Fig. S3 B) conforming the self-quenching as observed with NioIR-C. The photothermal transduction of NioIR783-C and NioICG-C was also evaluated following NIR laser irradiation, and as shown in Fig. S3 C temperature increment was observed in both of the encapsulated cyanine dyes.

To evaluate the mucoadhesive potential of nanoparticles, mucin binding assay was performed. Chitosan is a known mucoadherant natural polymer and presence of chitosan on niosome can significantly impart the mucoadhesive property to the nanosystem. This makes them a promising nanosystem for the photothermal treatment of breast cancer. As shown in Fig. 5 A, B a significant interaction of mucin was observed in NioIR-C when compared with NioIR, which is evident from the decline in unbound mucin absorbance. A fivefold increase in mucin binding efficacy was seen in NioIR-C when compared with NioIR.

The mucoadhesive potential of NioIR-C was further evaluated by a modified film adhesion assay as represented in schematic Fig. 6 A, B and Fig. S4 A-C. The fabricated artificial mucosa mimetic membrane is enriched with mucopolysaccharides which mimic cancer tumor environment [44]. The result shows that there was no significant interaction of mucosa mimetic membrane with IR dye and NioIR coated

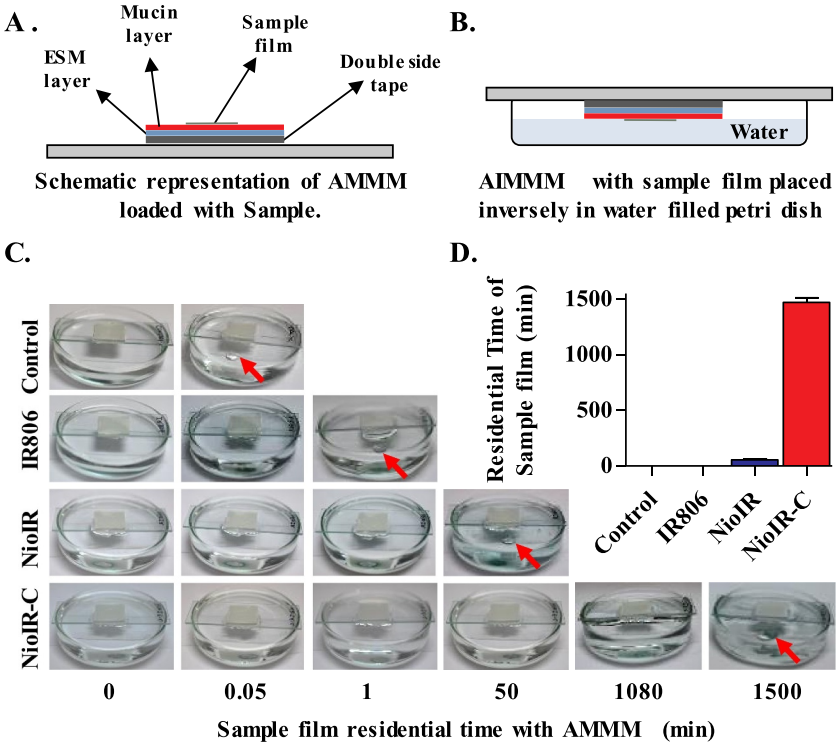

Fig. 6. Artificial mucosa mimetic membrane mucoadhesion assay; A. Schematic representation of AMMM loaded with sample film; B. Schematic representation of AMMM with sample film placed inversely in water filled petri dish; C. Photographic images of experimental set up after detachment of sample film; D. Bar graph for residential time of control, IR 806, NioIR, and NioIR-C.

films (Fig. 6 C,D). whereas, in case of NioIR-C, mucoadhesive interaction of NioIR-C coated film to the mucosa mimetic membrane was evident beyond 24 h (approx. 1500 min). A 30-fold increase was seen in NioIR-C when compared with NioIR. This mucoadhesive potential analysis also corroborates with mucin binding assay, thus confirming the mucin binding property of NioIR-C.

The biocompatibility of various niosome made up of span 20, span 40 and span 60 were evaluated on NIH 3 T3 cell line. All niosome exhibited biocompatibility up to 0.5 mg/ml. Span 40 niosome has exhibited higher biocompatibility when compared to span 20 and 60 (Fig. S5 A,B). The biocompatibility of IR 806 dye, NioIR and NioIR-C were assessed with normal cell lines (NIH 3 T3 and L929). It was observed that IR 806 dye showed 86–96% viability with normal cell lines. The NioIR-C and NioIR exhibited 75.45% and 61.27% cell viability with NIH 3 T3 cells whereas, 97.82% and 97.36% cell viability with L929 cells, respectively (Fig. 7A, B, S6). These findings were similar to the earlier literature reports suggesting the varying response in cytotoxicity of L929 and NIH 3 T3 cell line due to its sensitivity [45,46]. It is also reported that the difference in the cytotoxicity of these two cell lines could be due to metabolic activity [47]. L929 cell line is known to be active metabolically than NIH 3 T3, thus exhibiting less cytotoxicity. The chitosan coating on NioIR further aided in enhancing the biocompatibility of the nanosystem [48].

The intracellular uptake of IR 806 dye (Both in a free and encapsulated form) was evaluated in MCF-7 cancer cell line; it was observed that within 5 h of incubation a significant amount of IR 806 dye was taken up by cells in NioIR and NioIR-C treated groups. Four and two fold increase in the uptake was seen in NioIR-C and NioIR, respectively, when compared with IR 806 dye (Fig. 8 A,B)[49,50. The fluorescence microscopy analysis was also performed to evaluate the intracellular uptake of the nanosystem by the cancer cell lines (MCF 7). Nile red (model dye) was added to the nanosystem to visualize the intracellular uptake. As shown in Fig. 9, cells treated with Nile red entrapping niosomes coated with chitosan (NioIR-C) exhibited enhance fluorescence when compared with only dye and (NioIR) treated cell line. These findings are in accordance with the literature reports suggesting minimal uptake of sulfonated cyanine dyes by cancer cells [12].

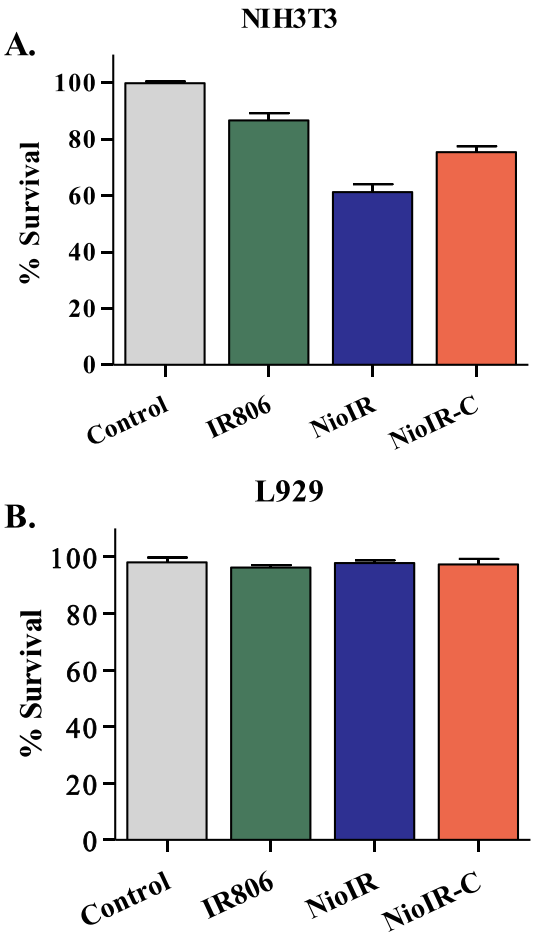

Fig. 7. Biocompability studies of IR 806, NioIR and NioIR-C. A. NIH3T3, B. L929.

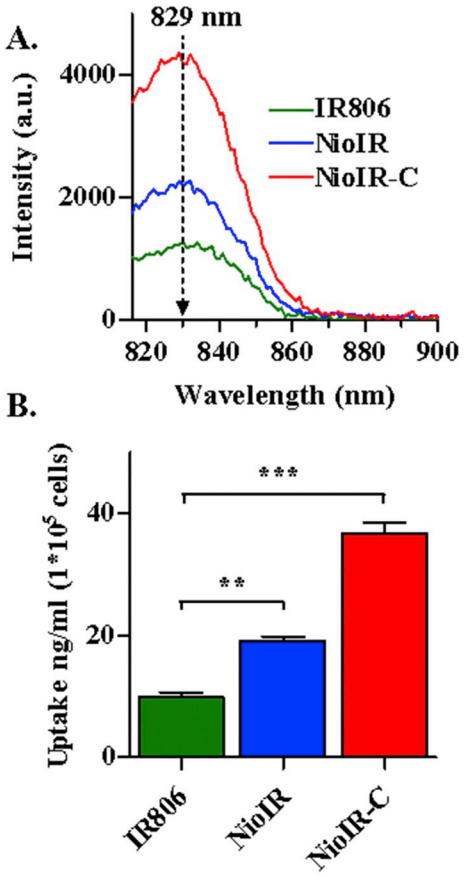

Fig. 8. Quantitative intracellular uptake in MCF 7 cell line. A. Fluorescence spectra of IR806 dye after 5 h of incubation with IR 806, NioIR, and NioIR-C.; B. Bar graph representing Intracellular uptake of IR 806, NioIR, and NioIR-C. IR 806 Uptake study using MCF-7 (**$p < .01$ and *** $p < .001$).

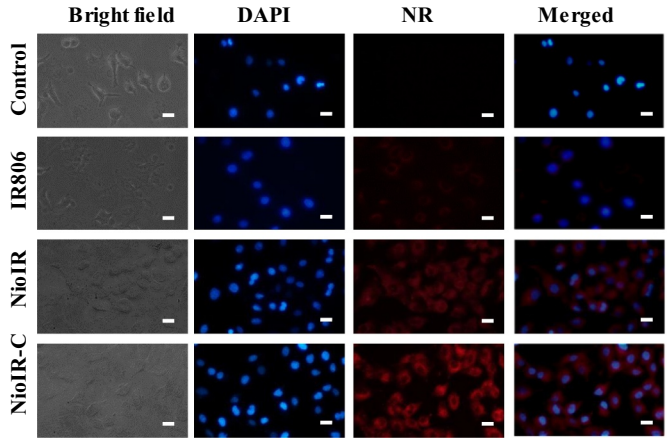

Fig. 9. Fluorescence microscopy imaging for intracellular uptake of IR 806, NioIR and NioIR-C in MCF-7 cell line. Nile red (NR) was used as model fluorescent dye. All the scale bars were 10 μm. (For interpretation of the references to colour in this figure legend, the reader is referred to the web version of this article.)

The enhanced intracellular uptake of IR 806 in NioIR and NioIR-C treated groups could be attributed to nanoparticle mediated delivery of the dye [50,51]. The surface charge of the nanoparticle plays a major role in enhancing cellular uptake. The chitosan coating, due to its $-NH_2$ bonds imparts positive charge on the surface of the nanoparticles enhances the uptake of nanoparticles through electrostatic interaction between the cell membrane and chitosan [52–56]. Hence, the higher

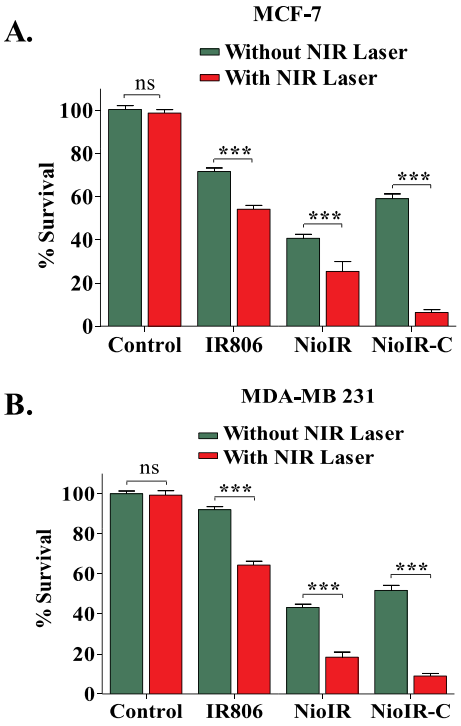

Fig. 10. Laser mediated cytotoxicity of IR 806 dye, NioIR and NioIR-C after 5 min of laser irradiation with breast cancer cell lines, A. MCF-7, B. MDA-MB 231 (*** $P < .001$).

uptake observed in the cancer cells treated with NioIR-C could be attributed to the presence of chitosan on the surface of the nanoparticles.

IR 806, NioIR, NioIR-C were then evaluated for the photothermal mediated cytotoxicity in breast cancer cell lines (MCF-7 and MDA-MB 231). As shown in Fig. 10 A,B, IR 806 dye treated group exhibited 71.65 ± 3.18% and 92.86 ± 2.32% cell viability in MCF-7 and MDA-MB 231, respectively. In NioIR treated group, 40.73 ± 3.95% and 42 ± 2.14%cells were viable in MCF-7 and MDA-MB 231, respectively. Whereas in NioIR-C treated group, 51.75 ± 3.89% and 58.05 ± 2.89% cells remained viable in MCF-7 and MDA-MB 231 cells, respectively. After 5 min of laser irradiation, a significant amount of cell death was observed in all the treated groups. Among all groups, NioIR-C showed a significant decline in cell viability to 92–96% in both MCF-7 and MDA-MB 231 cells, followed by NioIR, showing 70–82% cell death in MCF-7 and MDA-MB 231. However, the IR 806 dye treated group showed 34–48% of cell death in both MCF-7 and MDA-MB 231.

The live/dead fluorescence cell imaging revealed that cells treated with IR 806 dye, NioIR and NioIR-C cause selective damage to cancer cells at the site of laser irradiation (Fig. 11). This suggested that encapsulation of IR 806 dye in niosome coated with chitosan significantly enhances selective cytotoxicity as well as improves photothermal effect in breast cancer cells.

To further assess its effect on glycoproteins (Mucin) in MCF-7 cell monolayer, cells were treated with IR 806, NioIR and NioIR-C. A significant disruption of the monolayer was observed in cells treated with NioIR-C + Laser. This finding suggests that the NioIR-C were capable of adhering to the cell monolayer and inflicting localized damage upon laser irradiation (Fig. 12).

4. Conclusions

In summary, we have developed chitosan coated biodegradable non-ionic surfactant based bilayer vesicles (Niosome) entrapping IR 806 dye (NioIR-C). NioIR-C enhanced photothermal transduction efficacy of IR 806 dye and exhibited prolonged hyperthermia, which

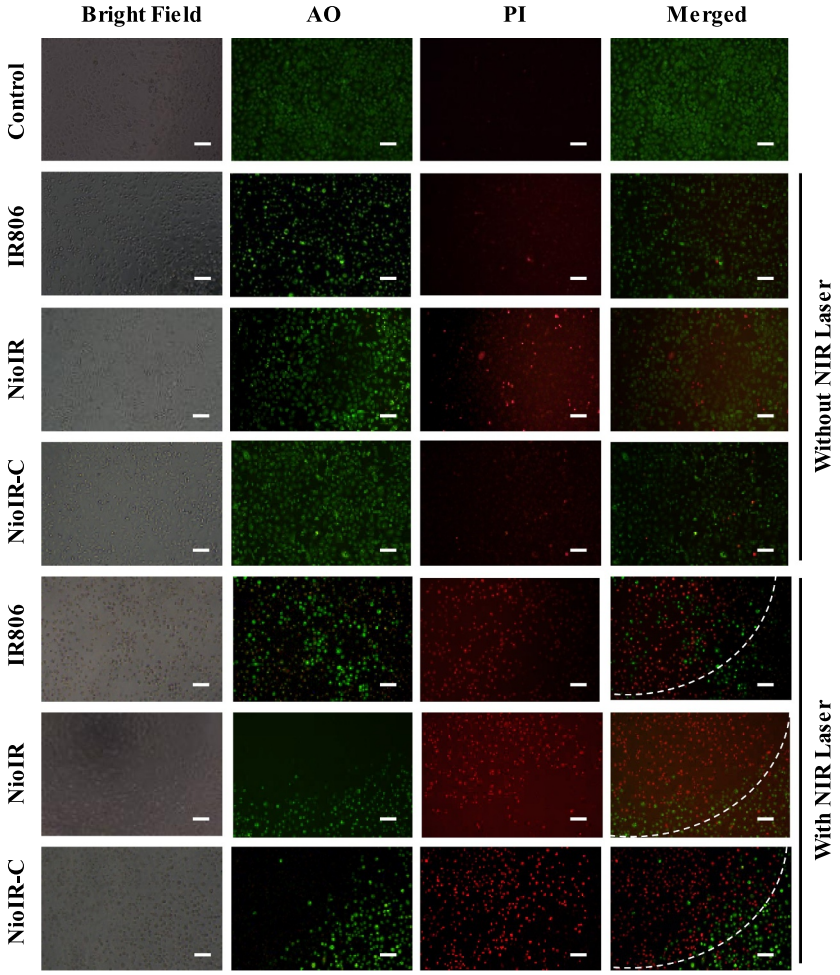

Fig. 11. Fluorescence based live dead assay in MCF 7 cell line after localized laser mediated cytotoxicity of IR 806, NioIR, and NioIR-C, using acridine orange and propidium iodide (AO/PI) staining. All the scale bars were 50 μm.

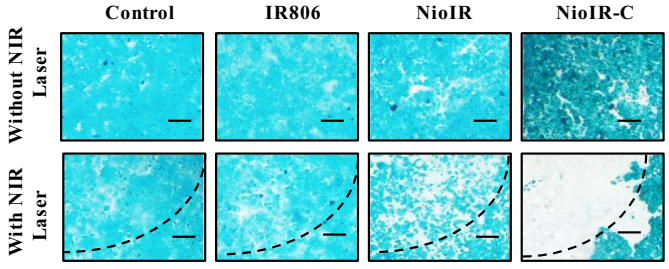

Fig. 12. Bright field microscopic imaging after laser mediated cytotoxicity in MCF-7 cell line monolayer with alcian blue staining. All the scale bars were 50 μm. (For interpretation of the references to colour in this figure legend, the reader is referred to the web version of this article.)

otherwise was not observed in IR 806 dye. NioIR-C were also found to exhibit efficient PTT and mucoadhesive potential. Thus NioIR-C can form an efficient nanosystem for selective killing of breast cancer cells.

Declaration of Competing Interest

None.

Acknowledgements

AJ would like to acknowledge the UGC (201516-RGNF-2015-17-SC-MAH-14156). Author SBA would like to thank the CSIR for SRF as financial support (09/1001(004)/2019-EMR-1). RJ would like to acknowledge the UGC (938/(OBC) (CSIR-UGC NET Dec.2016)) for financial support. AKR would like to acknowledge funding agencies DBT-BT/09/IYBA/2015/14, BT-NNT/28/1836/2017, MHRD-IMPRINT-4291, DST-INSPIRE/04/2015/00037 for their generous financial support.

Appendix A. Supplementary data

Supplementary data to this article can be found online at https://doi.org/10.1016/j.jphotobiol.2020.111901.

References

[1] J. Ferlay, I. Soerjomataram, R. Dikshit, S. Eser, C. Mathers, M. Rebelo, D.M. Parkin, D. Forman, F. Bray, Cancer incidence and mortality worldwide: sources, methods and major patterns in GLOBOCAN 2012, Int. J. Cancer (2015), https://doi.org/10.1002/ijc.29210.
[2] M.I. Nounou, F. ElAmrawy, N. Ahmed, K. Abdelraouf, S. Goda, H. Syed-Sha-Qhattal, Breast cancer: conventional diagnosis and treatment modalities and recent patents and technologies, Breast Cancer Basic Clin. Res. (2015), https://doi.org/10.4137/bcbcr.s29420.
[3] T.A. Buchholz, Controversies regarding the use of radiation after mastectomy in breast cancer, Oncologist (2004), https://doi.org/10.1634/theoncologist.7-6-539.
[4] A.M. Smith, M.C. Mancini, S. Nie, Bioimaging: second window for in vivo imaging, Nat. Nanotechnol. (2009), https://doi.org/10.1038/nnano.2009.326.
[5] Z. Bao, X. Liu, Y. Liu, H. Liu, K. Zhao, Near-infrared light-responsive inorganic nanomaterials for photothermal therapy, Asian J. Pharm. Sci. (2016), https://doi.org/10.1016/j.ajps.2015.11.123.
[6] H.J. Yoon, H.S. Lee, J.H. Jung, H.K. Kim, J.H. Park, Photothermally amplified therapeutic liposomes for effective combination treatment of Cancer, ACS Appl. Mater. Interfaces (2018), https://doi.org/10.1021/acsami.7b15996.

[7] M. Liu, P. Zhang, L. Deng, D. Guo, M. Tan, J. Huang, Y. Luo, Y. Cao, Z. Wang, IR780-based light-responsive nanocomplexes combining phase transition for enhancing multimodal imaging-guided photothermal therapy, Biomater. Sci. (2019), https://doi.org/10.1039/c8bm01524d.

[8] D.M. Valcourt, M.N. Dang, E.S. Day, IR820-loaded PLGA nanoparticles for photothermal therapy of triple-negative breast cancer, J. Biomed. Mater. Res. - Part A (2019), https://doi.org/10.1002/jbm.a.36685.

[9] C. Esposito, F. Del Conte, M. Cerulo, F. Gargiulo, S. Izzo, G. Esposito, M.I. Spagnuolo, M. Escolino, Clinical application and technical standardization of indocyanine green (ICG) fluorescence imaging in pediatric minimally invasive surgery, Pediatr. Surg. Int. (2019), https://doi.org/10.1007/s00383-019-04519-9.

[10] J.C. Kraft, R.J.Y. Ho, Interactions of indocyanine green and lipid in enhancing near-infrared fluorescence properties: The basis for near-infrared imaging in vivo, Biochemistry (2014), https://doi.org/10.1021/bi500021j.

[11] A. Lacroix, E. Vengut-Climent, D. De Rochambeau, H.F. Sleiman, Uptake and fate of fluorescently labeled DNA nanostructures in cellular environments: a cautionary tale, ACS Cent. Sci. (2019), https://doi.org/10.1021/acscentsci.9b00174.

[12] C. Agbavwe, M.M. Somoza, Sequence-dependent fluorescence of cyanine dyes on microarrays, PLoS One (2011), https://doi.org/10.1371/journal.pone.0022177.

[13] S.-L. Lin, Z.-R. Chen, C.A. Chang, Nd 3+ sensitized core-shell-shell nanocomposites loaded with IR806 dye for photothermal therapy and up-conversion luminescence imaging by a single wavelength NIR light irradiation, Nanotheranostics (2018), https://doi.org/10.7150/ntno.25901.

[14] P. Dogra, N.L. Adolphi, Z. Wang, Y.S. Lin, K.S. Butler, P.N. Durfee, J.G. Croissant, A. Noureddine, E.N. Coker, E.L. Bearer, V. Cristini, C.J. Brinker, Establishing the effects of mesoporous silica nanoparticle properties on in vivo disposition using imaging-based pharmacokinetics, Nat. Commun. (2018), https://doi.org/10.1038/s41467-018-06730-z.

[15] A. Yuan, J. Wu, X. Tang, L. Zhao, F. Xu, Y. Hu, Application of near-infrared dyes for tumor imaging, photothermal, and photodynamic therapies, J. Pharm. Sci. (2013), https://doi.org/10.1002/jps.23356.

[16] S. Luo, E. Zhang, Y. Su, T. Cheng, C. Shi, A review of NIR dyes in cancer targeting and imaging, Biomaterials (2011), https://doi.org/10.1016/j.biomaterials.2011.06.024.

[17] A. Suganami, T. Toyota, S. Okazaki, K. Saito, K. Miyamoto, Y. Akutsu, H. Kawahira, A. Aoki, Y. Muraki, T. Madono, H. Hayashi, H. Matsubara, T. Omatsu, H. Shirasawa, Y. Tamura, Preparation and characterization of phospholipid-conjugated indocyanine green as a near-infrared probe, Bioorg. Med. Chem. Lett. (2012), https://doi.org/10.1016/j.bmcl.2012.10.044.

[18] C.G. Alves, D. de Melo-Diogo, R. Lima-Sousa, E.C. Costa, I.J. Correia, Hyaluronic acid functionalized nanoparticles loaded with IR780 and DOX for cancer chemo-photothermal therapy, Eur. J. Pharm. Biopharm. (2019), https://doi.org/10.1016/j.ejpb.2019.02.016.

[19] Y.R. Zhang, R. Lin, H.J. Li, W. Ling He, J.Z. Du, J. Wang, Strategies to improve tumor penetration of nanomedicines through nanoparticle design, Wiley Interdiscip. Rev. Nanomed. Nanobiotechnol. (2019), https://doi.org/10.1002/wnan.1519.

[20] O. Trédan, C.M. Galmarini, K. Patel, I.F. Tannock, Drug resistance and the solid tumor microenvironment, J. Natl. Cancer Inst. (2007), https://doi.org/10.1093/jnci/djm135.

[21] L. Zhang, P. Hao, D. Yang, S. Feng, B. Peng, D. Appelhans, T. Zhang, X. Zan, Designing nanoparticles with improved tumor penetration: surface properties from the molecular architecture viewpoint, J. Mater. Chem. B (2019), https://doi.org/10.1039/c8tb03034k.

[22] M. Boegh, H.M. Nielsen, Mucus as a barrier to drug delivery - understanding and mimicking the barrier properties, Basic Clin. Pharmacol. Toxicol. (2015), https://doi.org/10.1111/bcpt.12342.

[23] H.H. Sigurdsson, J. Kirch, C.M. Lehr, Mucus as a barrier to lipophilic drugs, Int. J. Pharm. (2013), https://doi.org/10.1016/j.ijpharm.2013.05.040.

[24] A. Dumitru, A. Procop, A. Iliesiu, M. Tampa, L. Mitrache, M. Costache, M. Sajin, A. Lazaroiu, M. Cirstoiu, Mucinous breast cancer: a review study of 5 year experience from a hospital-based series of cases, Maedica (Buchar) 10 (1) (2015) 14–18.

[25] C.V. Rao, N.B. Janakiram, A. Mohammed, Molecular pathways: mucins and drug delivery in cancer, Clin. Cancer Res. (2017), https://doi.org/10.1158/1078-0432.CCR-16-0862.

[26] Y. Zubairu, L.M. Negi, Z. Iqbal, S. Talegaonkar, Design and development of novel bioadhesive niosomal formulation for the transcorneal delivery of anti-infective agent: in-vitro and ex-vivo investigations, Asian J. Pharm. Sci. (2014), https://doi.org/10.1016/j.ajps.2015.02.001.

[27] X. Ge, M. Wei, S. He, W.E. Yuan, Advances of non-ionic surfactant vesicles (niosomes) and their application in drug delivery, Pharmaceutics (2019), https://doi.org/10.3390/pharmaceutics11020055.

[28] G. Abdelbary, N. El-gendy, Niosome-encapsulated gentamicin for ophthalmic controlled delivery, AAPS PharmSciTech (2008), https://doi.org/10.1208/s12249-008-9105-1.

[29] F. Rinaldi, P.N. Hanieh, L.K.N. Chan, L. Angeloni, D. Passeri, M. Rossi, J.T.W. Wang, A. Imbriano, M. Carafa, C. Marianecci, Chitosan glutamate-coated niosomes: a proposal for nose-to-brain delivery, Pharmaceutics (2018), https://doi.org/10.3390/pharmaceutics10020038.

[30] A.-Z.M. Khalifa, B.K. Abdul Rasool, Optimized mucoadhesive coated niosomes as a sustained oral delivery system of famotidine, AAPS PharmSciTech (2017), https://doi.org/10.1208/s12249-017-0780-7.

[31] S.P. Singh, S.B. Alvi, D.B. Pemmaraju, A.D. Singh, S.V. Manda, R. Srivastava, A.K. Rengan, NIR triggered liposome gold nanoparticles entrapping curcumin as in situ adjuvant for photothermal treatment of skin cancer, Int. J. Biol. Macromol. (2018), https://doi.org/10.1016/j.ijbiomac.2017.11.163.

[32] K.M. El-Say, Maximizing the encapsulation efficiency and the bioavailability of controlled-release cetirizine microspheres using Draper–Lin small composite design, Drug Des. Devel. Ther. (2016), https://doi.org/10.2147/DDDT.S101900.

[33] A. Kumar, A. Kumar, Fabrication of eggshell membrane–based novel buccal mucosa–mimetic surface and mucoadhesion testing of chitosan oligosaccharide films, J. Mater. Res. 34 (2019) 3777–3786, https://doi.org/10.1557/jmr.2019.318.

[34] J. Van Meerloo, G.J.L. Kaspers, J. Cloos, Cell sensitivity assays: the MTT assay, Methods Mol. Biol. (2011), https://doi.org/10.1007/978-1-61779-80-5_20.

[35] A.R. Maity, A. Chakraborty, A. Mondal, N.R. Jana, Carbohydrate coated, folate functionalized colloidal graphene as a nanocarrier for both hydrophobic and hydrophilic drugs, Nanoscale (2014), https://doi.org/10.1039/c3nr05431d.

[36] L.L.Y. Chan, T. Smith, K.A. Kumph, D. Kuksin, S. Kessel, O. Déry, S. Cribbes, N. Lai, J. Qiu, A high-throughput AO/PI-based cell concentration and viability detection method using the Celigo image cytometry, Cytotechnology (2016), https://doi.org/10.1007/s10616-016-0015-x.

[37] L.J. Hronowski, T.P. Anastassiades, Detection and quantitation of proteoglycans extracted from cell culture medium and cultured cartilage slices, Anal. Biochem. (1988), https://doi.org/10.1016/0003-2697(88)90050-4.

[38] S.B. Alvi, T. Appidi, B.P. Deepak, P.S. Rajalakshmi, G. Minhas, S.P. Singh, A. Begum, V. Bantal, R. Srivastava, N. Khan, A.K. Rengan, The “nano to micro” transition of hydrophobic curcumin crystals leading to *in situ* adjuvant depots for Au-liposome nanoparticle mediated enhanced photothermal therapy, Biomater. Sci. (2019), https://doi.org/10.1039/C9BM00932A.

[39] S. Srinivasan, R. Manchanda, A. Fernandez-Fernandez, T. Lei, A.J. Mcgoron, Near-infrared fluorescing IR820-chitosan conjugate for multifunctional cancer theranostic applications, J. Photochem. Photobiol. B Biol. (2013), https://doi.org/10.1016/j.jphotobiol.2012.12.008.

[40] F.L. Tansi, R. Rüger, M. Rabenhold, F. Steiniger, A. Fahr, W.A. Kaiser, I. Hilger, Liposomal encapsulation of a near-infrared fluorophore enhances fluorescence quenching and reliable whole body optical imaging upon activation in vivo, Small (2013), https://doi.org/10.1002/smll.201203211.

[41] F.L. Tansi, R. Rüger, M. Rabenhold, F. Steiniger, A. Fahr, I. Hilger, Fluorescence-quenching of a liposomal-encapsulated near-infrared fluorophore as a tool for in vivo optical imaging, J. Vis. Exp. (2015), https://doi.org/10.3791/52136.

[42] Y.J. Gong, X.B. Zhang, G.J. Mao, L. Su, H.M. Meng, W. Tan, S. Feng, G. Zhang, A unique approach toward near-infrared fluorescent probes for bioimaging with remarkably enhanced contrast, Chem. Sci. (2016), https://doi.org/10.1039/c5sc04014k.

[43] J.R. Lakowicz, Principles of Fluorescence Spectroscopy, (2006), https://doi.org/10.1007/978-0-387-46312-4.

[44] B.T. Vu, S.A. Shahin, J. Croissant, Y. Fatieiev, K. Matsumoto, T. Le-Hoang Doan, T. Yik, S. Simargi, A. Conteras, L. Ratliff, C.M. Jimenez, L. Raehm, N. Khashab, J.O. Durand, C. Glackin, F. Tamanoi, Chick chorioallantoic membrane assay as an in vivo model to study the effect of nanoparticle-based anticancer drugs in ovarian cancer, Sci. Rep. (2018), https://doi.org/10.1038/s41598-018-25573-8.

[45] M.F. Maioral, Do C.N. Bodack, N.M. Stefanes, Á. Bigolin, A. Mascarello, L.D. Chiaradia-Delatorre, R.A. Yunes, R.J. Nunes, M.C. Santos-Silva, Cytotoxic effect of a novel naphthylchalcone against multiple cancer cells focusing on hematologic malignancies, Biochimie (2017), https://doi.org/10.1016/j.biochi.2017.06.004.

[46] M. Staszek, J. Siegel, S. Rimpelová, O. Lyutakov, V. Švorčík, Cytotoxicity of noble metal nanoparticles sputtered into glycerol, Mater. Lett. (2015), https://doi.org/10.1016/j.matlet.2015.06.021.

[47] J.C. Wataha, C.T. Hanks, Z. Sun, Effect of cell line on in vitro metal ion cytotoxicity, Dent. Mater. (1994), https://doi.org/10.1016/0109-5641(94)90025-6.

[48] S.F. Shi, J.F. Jia, X.K. Guo, Y.P. Zhao, D.S. Chen, Y.Y. Guo, T. Cheng, X.L. Zhang, Biocompatibility of chitosan-coated iron oxide nanoparticles with osteoblast cells, Int. J. Nanomedicine (2012), https://doi.org/10.2147/IJN.S34348.

[49] L.D. Mayer, M.B. Bally, P.R. Cullis, S.L. Wilson, J.T. Emerman, Comparison of free and liposome encapsulated doxorubicin tumor drug uptake and antitumor efficacy in the SC115 murine mammary tumor, Cancer Lett. (1990), https://doi.org/10.1016/0304-3835(90)90212-G.

[50] D.S. Shaker, M.A. Shaker, M.S. Hanafy, Cellular uptake, cytotoxicity and in-vivo evaluation of Tamoxifen citrate loaded niosomes, Int. J. Pharm. (2015), https://doi.org/10.1016/j.ijpharm.2015.07.041.

[51] H. Gogoi, R. Mani, R. Bhatnagar, A niosome formulation modulates the Th1/Th2 bias immune response in mice and also provides protection against anthrax spore challenge, Int. J. Nanomedicine (2018), https://doi.org/10.2147/IJN.S153150.

[52] S. Dyawanapelly, U. Koli, V. Dharamdasani, R. Jain, P. Dandekar, Improved mucoadhesion and cell uptake of chitosan and chitosan oligosaccharide surface-modified polymer nanoparticles for mucosal delivery of proteins, Drug Deliv. Transl. Res. (2016), https://doi.org/10.1007/s13346-016-0295-x.

[53] Y. Luo, Z. Teng, Y. Li, Q. Wang, Solid lipid nanoparticles for oral drug delivery: chitosan coating improves stability, controlled delivery, mucoadhesion and cellular uptake, Carbohydr. Polym. (2015), https://doi.org/10.1016/j.carbpol.2014.12.084.

[54] A. Alalaiwe, P. Carpinone, S. Alshahrani, B. Alsulays, M. Ansari, M. Anwer, S. Alshehri, A. Alshetaili, Influence of chitosan coating on the oral bioavailability of gold nanoparticles in rats, Saudi Pharm. J. (2019), https://doi.org/10.1016/j.jsps.2018.09.011.

[55] K. Tahara, T. Sakai, H. Yamamoto, H. Takeuchi, N. Hirashima, Y. Kawashima, Improved cellular uptake of chitosan-modified PLGA nanospheres by A549 cells, Int. J. Pharm. (2009), https://doi.org/10.1016/j.ijpharm.2009.07.023.

[56] P. Foroozandeh, A.A. Aziz, Insight into cellular uptake and intracellular trafficking of nanoparticles, Nanoscale Res. Lett. (2018), https://doi.org/10.1186/s11671-018-2728-6.